Bioscience and Bioengineering
Vol. 1, No. 4, 2015, pp. 94-105
http://www.aiscience.org/journal/bio

Applied Inverse Methods for Optimal Deformation of Lumbar Artificial Disk/Implants with Numerical Reuleaux Method and 3D Voxelization-Computational Simulations

Francisco Casesnoves*

Computational Bioengineering, International Institute of Informatics and Systemics, Orlando, Florida State, USA

Abstract

Lumbar artificial implants/disks experiment material deformations during the biomechanical loads/movements that are acting dynamically on the lumbar spine, e.g., flexion, extension, lateral flexion and torsion. During this biomechanical process disks and vertebras, (each spine part as a whole in general) move around an Instantaneous Rotation Center (IRC, 3D) or an Instantaneous Axis of Rotation (IAR, 2D). During extreme conditions of physical effort, the angles of IRC/IAR are enforced until reaching the maximum of their anatomical-physiological capabilities, with additional work-load for muscles, tendons, cartilage, and surrounding tissues. We carried out geometrical-mathematical-approaches to determine optimal deformation, given a selected IRC/IAR, which was chosen different from the non-deformed solid IRC/IAR, and find out the implant physical-geometrical variables linked to that obtained deformation. Voxelization of the implant in 3D constitutes the basis of this new contribution. Computational-Numerical Method was the inverse geometrical algorithms of Numerical Reuleaux Method (NRM), based on previous publications/algorithms. Once the optimal deformation was determined, the numerical 3D fitting to a nonlinear polynomial for the stress and strain was calculated. Initial results agreed to formal NRM with useful data of contact mechanics stress/strain equations/parameters and distribution/magnitudes, all complemented with matrix algebra numerical formulation and radiological experimental data. Bioengineering applications and Radiology-geometrical results, both for manufacturing design and clinical improvements were presented.

Keywords

Lumbar Artificial Implants, Reuleaux Method (RM), Numerical Reuleaux Method (NRM), Contact Mechanics, Instantaneous Rotation Center (IRC), Optimization, Numerical-Geometrical Methods

Received: April 10, 2015 / Accepted: August 13, 2015 / Published online: September 25, 2015

1. Introduction

Lumbar artificial implants have became an efficacious surgical alternative for spinal fusion in recent years. This type of surgery is indicated when Low Back Pain (LBP) and natural disk degeneration diseases do not show objective/subjective relief after conventional medical/surgical/physical treatment (e.g., pharmacological, quiropractic, physical therapy, laser, disk hernia partial surgical removal, and a large number of medical-surgical treatments available currently in proper clinical services). The surgical/medical objective of the lumbar artificial disk is to restore the basic biomechanics of lumbar spine, without sympthoms of LBP, and provide the patient with strong psychological self-confidence of his cure and movement-restoration status. Currently, however, it is not extensively proven the better surgical outcome over the classical spinal fusion technique, although wide literature reviews based on Bayesian Methods asserted/indicated that

* Corresponding author
E-mail address: casesnoves.research.emailbox@gmail.com

the probability for artificial disk replacement (ADR) being better than spinal fusion was 79% [Ref 24]. The most frequent movements in lumbar spine are flexion/extension, apart from axial rotation and lateral bending. The biomechanics of flexion/extension is defined by a Torque, which is physically equal to the time-derivative of the angular moment, and performed anatomically principally by a group of trunk muscles. Intervertebral ligaments share a part of the mechanical forces linked to vertebral movements, since these groups of ligaments are mechanically strong. Modeling intervertebral ligaments, therefore, is important to optimize the necessary forces to make an anatomical-physiological movement and also for disk surgery during the distraction of consecutive vertebras.

We carried out, in previous contributions, several intervertebral ligaments modeling, to determine these distraction/extension forces (about several hundred N) and used a non-linear exponential model [Refs 1,3, Casesnoves, 2008, 2011]. Consequently, both physical parameters, torque and moment, modulated by muscle, ligaments and tendon forces, are around the Instantaneous Rotation Center (IRC) in 3D or the Instantaneous Axis of Rotation (IAR) in 2D. Other authors [Ref 28], consider to measure the Instantaneous Helical Axis (IHA), because the pure rotation could happen simultaneously with a translation, generating a helicoidal movement [Ref 28].

The IRC natural has not a fixed and equal location for each type of movement in the natural disk, it is rather an IAR (instantaneous axis of rotation) when pure flexion, extension or lateral bending movements are performed. Furthermore [Fig 1 from Ref 27], the IAR and therefore the IRC, can set a different positioning depending on the angular range of the movement [Figs 1, 2]. The IRC of a lumbar disk implant is important because after surgery, sub-optimal positioning can cause wrong IRC setting, ligaments alterations, and in addition, changes/damage in vertebral facets joints could also happen. If sub-optimal positioning of the ADR occurs, spinal movements can be affected, with change(s) in the normal movements of flexion, extension, lateral bending, torsion, etc.The surrounding tissues could be damaged, and severe LBP in the patient could appear [Ref 3]. In other words, both the natural and artificial disks, together with adjacent vertebrae, ligaments, and muscles, constitute a biomechanical sub-unit, whose mechanical functionality depends on each and every part of this sub-unit, and forms an element of the whole spine biomechanical unit. The complete movement of the spine (lumbar, thoracic and cervical), is a rather complicated mechanobiological system because, additionally, the natural loads/torques/moments involved in this movement (stand-up, walk, or run), present high physical magnitude orders. That is, body weights and ligament/muscles forces are exerted over small surfaces (vertebral plates) and create a high physical pressure magnitude and forces-distribution. Therefore, for all these reasons, to preserve/approximate the IRC/IAR of the implant to the natural intervertebral disk is essential [Refs 5, 6, 13-19].

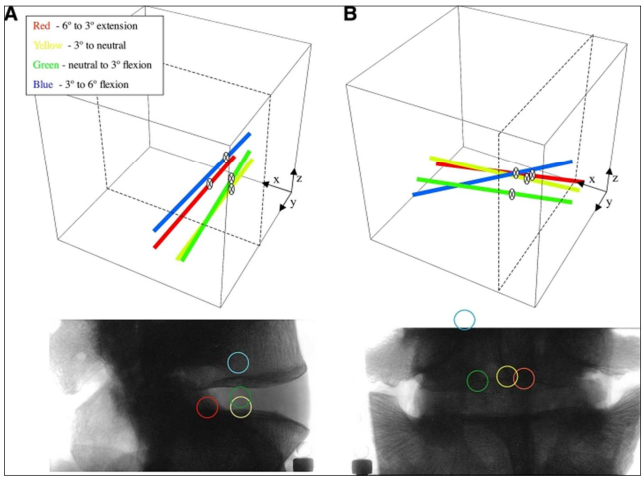

Fig. 1. [excellent sketch from Ref 27, Rousseau, M-A, Bradford, DS, Hadi TM, Pedersen KL, and Lotz JC, Springer]. We observe how the IAR in (A) Flexion-Extension, and (B) Lateral Bending changes its position depending not only on movement type, but also on angular rage of the movement.

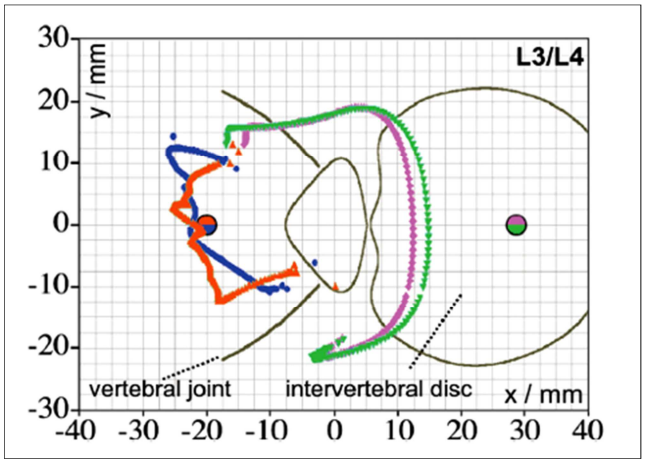

Fig. 2. [excellent sketch from.Wachowski, Hawellek T, Hubert J, Lehman A, Mansour M, Dumont C, Dorner J, Raab B, Kubein-Meesenburg D, Nagerl H. 'Migration of the instantaneous axis of motion during axial rotation in lumbar segments and role of the zygapophysial joints'. Acta of Bioengineering, Ref 28] .Sharp proven variation of the IAR (IHA, Instantaneous Helical Axis in this publication), after resection of important intervertebral ligaments. This demonstrates the close biomechanical link between the exerted forces by intervertebral ligaments and the IRC positioning of the lumbar segment. A lumbar segment is a sub-unit of the spine unity and therefore the IRC/IAR of the disk is included into the variation of the lumbar segment as a whole.

In this way, the bioengineering design of artificial lumbar disks takes into account as important point to resemble in material-physics parameters and functionality the IRC of the natural disk (as much as possible, using optimal approximations). Approximations/constructive methods are carried out numerically (although analytic resolution is

always considered) beginning from the simplest formulation towards refinements and improvements/changes in the algorithms [Refs 10, 11, 12]. In general, we can approach the anatomical locus of the lumbar-disk/implant IRC/IAR within the posterior third part of the natural disk [Refs 16, 29].

The biomechanical reason for this objective, as said, is to reproduce physically the natural movement of the lumbar spine, given the high loads (about several hundred N) that this part of the spine bears, and avoid any post-surgical LBP. The lumbar spine natural disk experiments an asymmetric variation of shape during flexion/extension. In flexion, the anterior part is compressed (compression muscular forces) and the posterior one is/could be extended (extension tissue-forces). Both flexion/extension movements are around the IRC/IAR. This is the initial physical parameter that determines the aim of this contribution using Inverse Problems Theory. The bioengineering design of lumbar artificial disks is carried out using a forward-problem mathematical method, usually.

However, mathematically is more accurate and practical to deal this industrial problem using inverse methods (IP) [Refs 2, 6]. That is, fix the desired IRC and obtain by inverse calculations the corresponding deformation of the implant. Then, manufacture the implant with appropriate materials (polymers, mixed-polymers, composites, mixed-composites, or others usually) that could provide exact/approximately this deformation and IRC. Numerical Reuleaux Method is a useful algorithm to perform this objective with non-linear optimization methods and convenient computational simulations. Therefore, in this contribution, a primary approach to deal this biomechanical problem/method was developed with physical-mathematical analysis, geometry, and numerical simulations. In Figures 3, 4, the lumbar flexion with small lateral bending algorithm is developed (3D), since extension is approximately the opposite movement, although biomechanical forces/muscles-acting are different. The rational objective is to obtain formulation for the non-linear inverse elastic modulus in a polynomial numerical fitting. These parameters are linked to stress and strain. Strain gives the optimal deformation for the selected IRC of the implant. Strain and Stress parameters obtained by inverse methods are linked to the implant materials characteristics. Coordinate Systems are essential to develop this method. A suitable choice for them can configure the problem simple and mathematically easy for calculations/simulations. Therefore, to deal the problem at first, approximations are convenient. Further development involves more complicated refinements for all the mathematical framework. We showed an example of lumbar artificial disk manufactured with polymeric materials (Compliant Artificial Disk, Figs 6, 7).

In previous publications, only 2D-pixel simulations were approximated and developed [Refs 5, 6]. In this continuing contribution we developed and detailed both computational techniques for a 3D voxelization and simulation and numerical data obtained using appropriate software.

In summary, we presented in this recent publication a mathematical computational method for inverse calculation of the IRC and deformation, 3D, of an artificial disk, with numerical determination of the stress/strain equation(s) based on that obtained deformity. Other types of artificial disks, (e.g., ball-and-socket, mixed designs, etc) can obtain improvements in biomechanical design by using this inverse method with/without variations. Results were shown both in geometrical sketches and numerical tables for sharp learning. A complementary series of experimental radiological imaging and geometrical data is shown. These radiological images are both geometrical simulations with RX machines at lab, and real clinical images *in vivo* of implants with patients after lumbar disk replacement surgery.

2. Mathematical-Geometrical Method (I)

The Coordinate System at initial position is X axis in antero-posterior direction, and Y axis in at cranial-caudal direction.After flexion angle, θ, (see results tables), we get the system rotated an angle θ and a coordinate system also rotated (2D) just that angle (X', Y'), Figs 3, 4, 8. Flexion velocity defines an angular velocity at initial position (vertical spine) we suppose Equations 1-4 conditions, and at final position we get different magnitudes of stress and strain depending of the rotation angles in Equations 1-5. On Equations 1-5 and Figures 3, 4, 8, we show a basic sketch about the coordinate system in lumbar spine flexion Formulation is according to these coordinates. Parameters A are the surfaces of forces application of the implant.

We derivate the stress respect to time. And integrate supposing angular velocity of flexion angle θ constant. All this formulation constitute a primary approximation. Torque and angular moment can be obtained from these formulas. The basic formula that relates stress to strain with Young Modulus is, $\sigma = E \times \varepsilon$. But this linear relation is not suitable for the polymeric (or similar, e.g., composites, mixed polymer;composites, etc) material of the implant. Therefore, we carry out a simple polynomial approximation [Matrix Algebra Formulation 1] of forces application of the implant. The rotation matrix in 2D reads,

2D Rotation Matrix

$$\begin{pmatrix} x' \\ y' \end{pmatrix} = \begin{pmatrix} \cos\theta & -\sin\theta \\ \sin\theta & \cos\theta \end{pmatrix} \times \begin{pmatrix} x \\ y \end{pmatrix} \; ; \qquad \text{Eq (1)}$$

and we define the angular velocity of flexion,

$$\dot{\theta} = \frac{d\theta(t)}{dt} \cong \frac{\Delta\theta(t)}{\Delta t} = |\vec{\omega}| \ ;$$

$$with \ \Delta t = t_\theta - t_0 \ ; \qquad \text{Eq (2)}$$

a simple setting of initial and final positions,

$$\sigma_X = \frac{|Load|}{A\,(Surface)} \ ; \quad \sigma_Y = 0 \ ;$$

$$\sigma_{X_1} = \sigma_X \cos\theta \ ; \quad \sigma_{X_1} = \sigma_{Y_1} \sin\theta \ ; \qquad \text{Eq (3)}$$

the forces distribution,

$$F_{X_1} = A_1 \times \sigma_{X_1} \ ;$$

$$F_{Y_1} = A_2 \times \sigma_{Y_1}$$

and we carry out a few differential approximations,

$$\frac{d\sigma_{X_1}}{dt} = \sigma_X\ (constant) \times \cos\theta \ \frac{d\theta}{dt} = \sigma_X \cos\theta \ |\vec{\omega}|$$

$$approximation - integration, \quad \int_{X_1}^{X} d\sigma_{X_1} = \int_{t_0}^{t} \cos\theta \ |\vec{\omega}| \ dt \ ; \qquad \text{Eqs (4)}$$

now we develop the main equation in 3D,

$$\begin{pmatrix} \sigma_{X1} \\ \sigma_{Y1} \\ \sigma_{Z1} \end{pmatrix} = \begin{pmatrix} \cos\alpha\cos\theta & -\sin\theta & \sin\alpha\cos\theta \\ \cos\alpha\sin\theta & \cos\theta & \sin\alpha\sin\theta \\ -\sin\alpha & 0 & \cos\alpha \end{pmatrix} \times \begin{pmatrix} \sigma_X \\ \sigma_Y \\ \sigma_Z \end{pmatrix}; \text{ Eq (5)}$$

We applied alpha-angle around Y (flexion) and theta-angle around Z (lateral flexion), all according to Tables 5, 7. The development of 3D Equations like Eqs 2, 3, 4, and 5 will be equal but in 3D with two angular velocities, three forces distribution, and two integral approximations. The difference is that the initial values are all null with exception of sigma-z (in Eqs (3,5) we deal with initial loads, Table 1). The initial load/surface, in 2D it was sigma-x. We applied here in the vector of rigth side of matrix equation the simulation loads, Table 1, and then we obtained the three loads distribution after rotation in 3D, Table 5. These final loads are divided by respective surfaces of voxels, and implemented in numerical software to obtain a polynomial fitting using deformation values (Eqs 5, 7).

3. Mathematical-Geometrical Method (II)

In this section we detail the mathematical development that was carried out to perform the voxelization/simulations both programming and geometrical techniques. We applied the Exact Inverse Method from [Ref 6], and set the linear system of equations with the IRC fixed to obtain the corresponding deformations. Then we remind from [Ref 6] the 3D optimization formulas for the bisecting Reuleaux planes, which are used initially to determine the natural IRC, directly taken from [Ref 6],

$$A_1 x + B_1 y + C_1 z = -D_1$$

$$A_2 x + B_2 y + C_2 z = -D_2$$

$$A_3 x + B_3 y + C_3 z = -D_3 \qquad \text{Eq (6)}$$

This is the linear system of equations for the bisecting planes, that can be used for a non-deformed solid or for a voxel of a deformed-solid. When the rotation angle approaches to zero, and therefore the movement is almost a translation, these planes can be almost parallel, therefore the coefficients of linear system are almost proportional, and the matrix of the system is either almost null or singular. This is a mathematical problem that can be resolved with a number of numerical and ill-posed solutions/methods, and has been explained in previous contributions of Numerical Reuleaux Method. Subsequently, for the deformed-solid inverse problem, once the selected IRC is chosen, the linear system is re-set to determine the optimal deformations. That is, directly taken from [Ref 6], the linear system reads,

$$A_1\,(\epsilon_1) \ x_{selected} + B_1\, y_{selected} + C_1\, z_{selected} = -D_1\ (\epsilon_1)$$

$$A_2\ x_{selected} + B_2\,(\epsilon_2)\ y_{selected} + C_2\ z_{selected} = -D_2\ (\epsilon_2)$$

$$A_3\ x_{selected} + B_3\, y_{selected} + C_3\,(\epsilon_3)\, z_{selected} = -D_3\ (\epsilon_3) \qquad \text{Eq (7)}$$

And the epsilons are the arbitrary deformations that can be determined, since the IRC is selected beforehand. In other words, we can set the deformations as we select them, at any A,B, or C coefficient of any linear equation (which is transformed in non-linear after the inclusion of epsilon). A large amount of data obtained with this method is shown in Table 5, from [ref 6]. In general, there are two methods, the numerical optimization of the multiobjective function, and the algebraic determination (computationally, that is a simple resolution of a linear system with appropriate subroutines) of the above linear/non-linear system. The deformations can be set arbitrarily in Eq (7).

We followed this algebraic method instead to minimize an objective function in L_2 or L_1 norms (for 2D see Eqs (8). Results are shown in Tables 5, 6, 7 with corresponding errors. The formal Reuleaux intersection points formulas in 2D, intersection of Reuleaux Segments in 2D (for sharp learning but not applied on 3D bisecting planes), are formulas directly taken from [Ref 6], Eqs 8 and 9, and read,

$$Y_{intersection} = \left(\frac{x_i' - x_i}{y_i - y_i'}\right) \times X_{intersection} + \frac{(y_i^2 - y_i'^2) - x_i'^2 + x_i}{2 \times (y_i - y_i')} \; ; \quad \text{Eqs (8)}$$

$$X_{intersection} = \frac{\left(y_i^2 - y_i'^2\right) - \left(x_i'^2 - x_i^2\right) - a}{b - \left(\frac{x_i' - x_i}{y_i - y_i'}\right)} \; ;$$

with

$$a = \frac{\left(y_j^2 - y_j'^2\right) - \left(x_j'^2 - x_j^2\right)}{2 \times \left(y_j - y_j'\right)} \; ; \; and$$

$$b = \frac{x_j' - x_j}{y_j - y_j'}$$

Where i and j are the two points selected to trace Reuleaux segments for each pixel/voxel Two terms of the Objective Function

$$w_1 \| X_{selected} - X(\varepsilon_1) \|_2^2 + w_2 \| Y_{selected} - Y(\varepsilon_2) \|_2^2 \; ; \quad \text{Eqs (9)}$$

In the following Figure 3, it is sketched the type or 3D rotations carried out for flexion with small angle of lateral bending

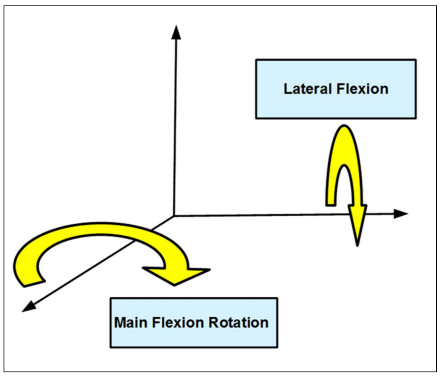

Fig. 3. Basic Sketch of simulations in 3D. We designed a lumbar flexion with a lateral flexion. Of we choose pure flexion, we are simulating in 2D and obtaining an IAR instead a IRC [ref 6].

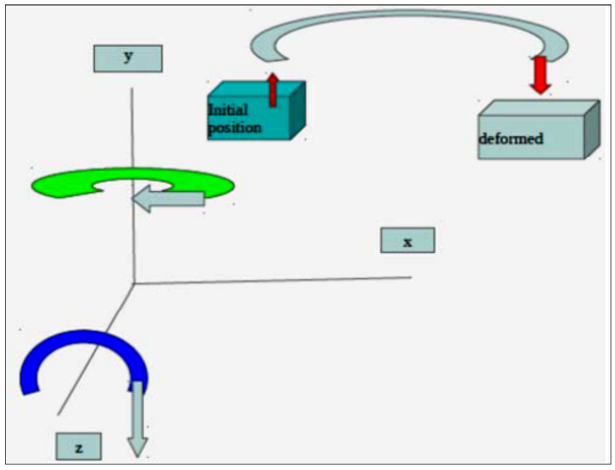

Fig. 4. Basic Sketch of simulations in 3D. We designed a lumbar flexion with a lateral flexion. Of we choose pure flexion, we are simulating in 2D and obtaining an IAR instead a IRC [ref 6].

For primary 2D inverse simulations, the artificial disk shape is approximated to a parallelepipedic volume of dimensions a,b,c.Then, A_1 = ab and A_2 = bc Stress and Strain Forces distribution (2D), are as given in Mathematical Development Section, carried out by Inverse Mathematical Methods. Data is taken from [Ref 6] directly (Exact 2D Inverse Deformations Table). Loads are taken from the literature (from 78 to 488 N) simulated according to increasing flexion angle, Table 1, from 20 to 50 degrees. IRCs are applied from Table 1 with different values for angle loads. Primary analysis was done setting intervals or loads, Table 6. The polynomial, for example in 2D, is chosen as second-degree one, namely,

$$\sigma_{X_i} = f(\delta_{ix}) = p(0)_{X_1} + p(1)_{X_1} \times \left(\frac{\delta_{1x}}{L_x}\right) + p(1)_{X_1} \times \left(\frac{\delta_{1x}}{L_x}\right)^2 \; ;$$

$$\sigma_{Y_i} = f(\delta_{iy}) = p(0)_{Y_1} + p(1)_{Y_1} \times \left(\frac{\delta_{1y}}{L_y}\right) + p(1)_{Y_1} \times \left(\frac{\delta_{1y}}{L_y}\right)^2 \; ; \quad \text{Eqs (10)}$$

Table 1. Loads applied in flexion taken from [ref 8 general].These loads were chosen,citing the reference description, in an attempt to mimic those that the lumbar spine supports in a person weighing between 70 and 80 kg. In our case, we took these loads at initial position horizontal, resembling the flexion initial force, which is transformed into axial compression during the flexion movement. Since this is a primary simulation to set the modeling towards improvements, the main interest was about using series of realistic loads applied for *in vitro* experimental.

Simulation loads for flexion			
Flexion Angle for α,θ	**Load (N)**	**IRC natural**	**IRC selected (all of Table 5)**
30/40. 40/30	78	(1,1,1)T	(1.5,1.5,1.5)T (1.4,1.4,1.4)T
30/40. 40/30	181	(1,1,1)T	
30/40. 40/30	282	(1,1,1)T	
30/40. 40/30	385	(1,1,1)T	
30/40. 40/30	488	(1,1,1)T	
Comments	Increasing value parallel to increasing angle	Translation of all the voxels from (0,0.0) to (1,1.1) according to [refs 6,7]	For polynomial fitting average values were selected for each voxel

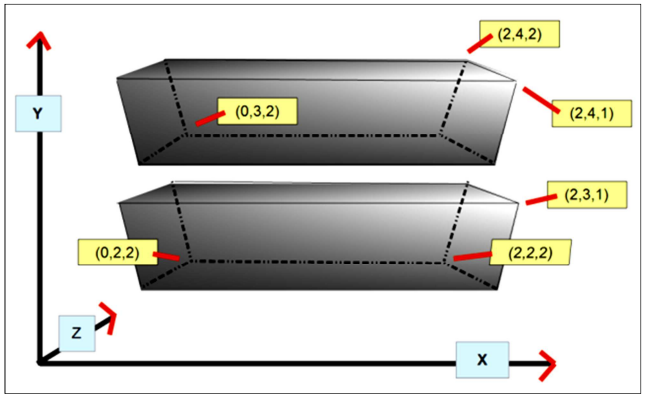

Fig. 5. Basic Sketch of voxelization in a tetrahedrical geometry for simulations. We specify tetrahedrical since the tetrahedral is chosen within the parallelepipedic voxel. Selected points are pictured, and 3D voxels images are separated for better learning. Initially, as a primary simulation in 3D, we are not too much precise about the exact equality between the disk volume and these voxel volumes. What is important is setting the IP and obtain accurate values of rotations/deformations.

In these Tables 2-7, the basic polynomial fitting that has been programmed with corresponding data to obtain mathematical formulation for stress/strain functions, with details of Matrix Numerical Algebra, 2D and 3D. There are a series of possible numerical different approximations, however. Numerical Approximations are related to material characteristics previously determined.

Table 2. Table-Description of programming subroutines and calls. In general, at this stage of study, programming is not complicated and further developments will require more optimization methods/programming.

Freemat Subroutines For Polynomial Fit	
Subroutine name	**Programming call**
polyfit	p=polyfit (x,y,n) x,y input data vector,n polynomial degree. Errors, Residuals, and other data can be obtained.
FITFUN	[xopt, yopt]=fitfun (fcn, xinit, y, weights. Tol, params...) fcn is the name of the function and xinit the initial guess (numerical figure)

The matrices [Matrix Algebra Formulation 1], show the numerical method carried out to develop the inverse problem. In other words, we select a convenient IRC for the implant, then, we obtain the optimal deformation, and finally with those data, the inverse problem is completed determining the optimal equation for stress-strain material parameters.

The development in 3D is according to voxels Figure 5 and initial and final points of Tables 6-7. The 3D matrices of Matrix Algebra Formulation 1 give the stress and strain numerical method for sharp learning.

4. Computational Simulations/Software and Numerical Results

Polynomial fitting is not a complicated optimization method since there are several subroutines that can be used to carry out this technique. It was selected this model because it is a primary approximation and the intention was to obtain a simple equation for stress and strain to proceed for further refinements in next stages.

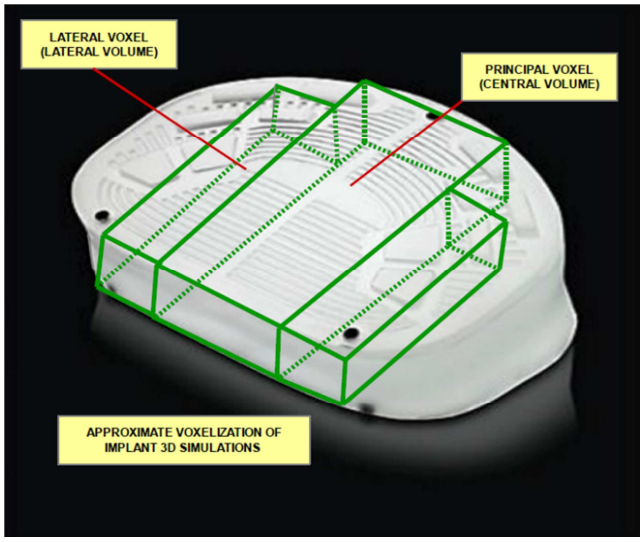

Fig. 6. Approximations for voxelization of the artificial lumbar disk to set the 3D simulations numerically for inverse determination of IRC (3D). The complete volume of the disk is almost covered, so the 3D simulation data could be approximated to the whole disk dynamics. We set 3 voxels for the most part of this volume of the disk, and next contributions will share all the resting wings-volume with 5 voxels. Note that the dark points over the disk surface correspond to radiological markers (60% tantalum composition after experimental optimization, [Ref 9]) that can be used during/after surgery to obtain an optimal setting of the disk. Sub-optimal position of the disk after operation could yield to paresthesias, severe radicular/disk pain, mobility difficulties, and in the long term increase of the biased position of the disk.

The basic polynomial fitting that has been programmed to obtain mathematical formulation for stress/strain functions is based on Freemat subroutines. There are a series of possible numerical different approximations, however. We consider also that Numerical Approximations are related to material characteristics previously determined, because it is previously determined for each material, e.g., polymers, composites, mixed polymers-composites, the approximated equations defining the proper physical parameters. The matrix shows the numerical method carried out to develop the inverse problem. In other words, we select a convenient IRC for the implant, then, we obtain the optimal deformation, and finally with those data, the inverse problem is completed determining the optimal equation for stress-strain material parameters. Polyfit is very

simple and fitfun has several alternatives.

5. Discussion and Conclusions Clinical-Design Bioengineering Applications

Mathematically it is possible to apply inverse methods to select a desirable IRC for a lumbar spine implant using the Numerical Reuleaux Method. The most important data are the values obtained for implant deformation. With these values we can carry out a non-linear optimization method to obtain the appropriate physical characteristics of the material of the implant. The implants that theoretically could take advantage of this method could be artificial disks of any type, compliant, ball and socket, mixed types, etc. are Coordinate systems are essential (2D, 3D) to make the problem resolvable. Numerical simulations can be extended to 3D towards getting better biomechanical results. Experimental Optimization of the mathematical results obtained by computational simulations constitute the final stage for lumbar artificial disk implant design. For future contributions, it is convenient to extend the Numerical Reuleaux Method towards a study of the applications in biomechanics of the Helicoidal Axis and related physical-geometrical concepts, [Ref 28].The reasons are that other researchers consider rationally to measure the Instantaneous Helical Axis (IHA), since the pure rotation could happen simultaneously with a translation, generating an helicoidal movement [Ref 28].

Fig. 7. A compliant artificial disk manufactured with polymers and composites and radiological markers that can be used for imaging position determination [Ref 9]. It was proven mathematically/simulations [Casesnoves, 4, 5, 6, 8, 9], that the IRC of this implant can be approximated with radiological imaging techniques using the Numerical Reuleaux Method.

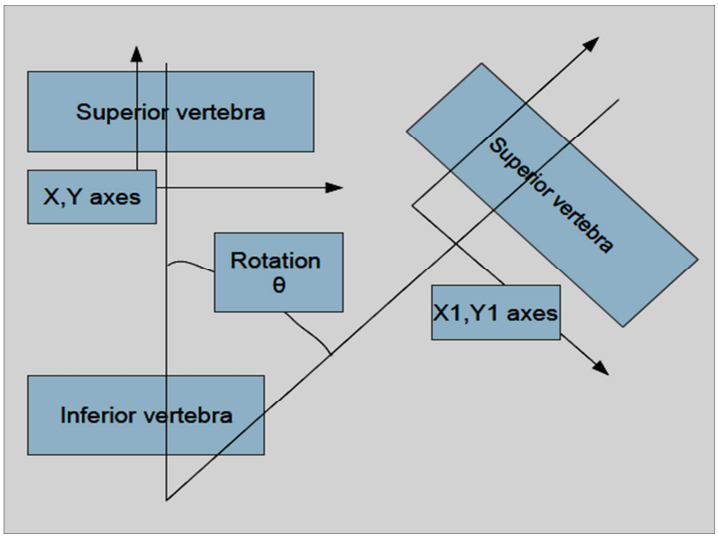

Fig. 8. 2D Coordinates System for movement for the numerical simulation of approximated IRC after rotation+deformation. This picture gives a geometrical idea in 2D, to be complemented in 3D by Figs 3, 4, 5.

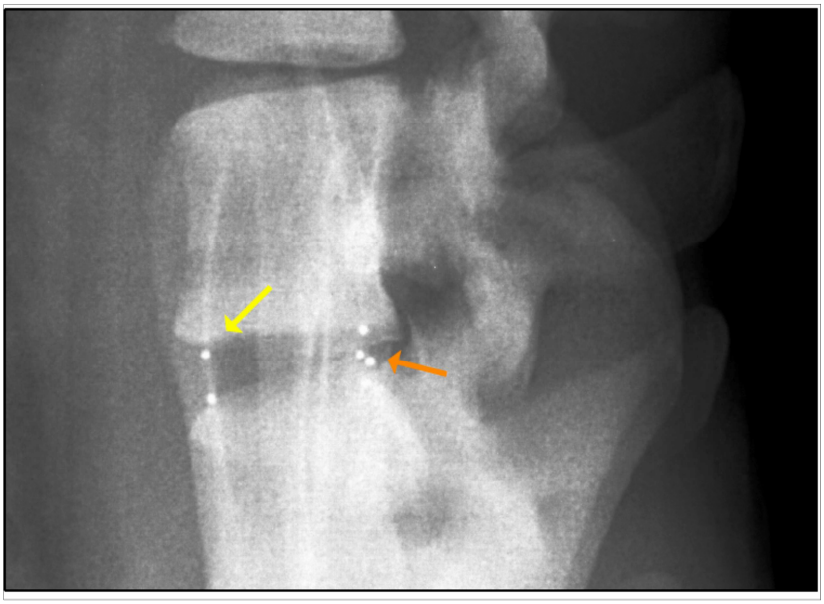

Fig. 9. Real Post-Implant-Surgery Radiological Position of Implant Before Flexion with Radiological Markers. A compliant artificial disk manufactured with composites and polymers and its radiological lateral image (contrast inverted, blank is black and viceversa) before flexion, Anterior markers,yellow arrow, posterior orange ones. Level is L3-L4 articulation, with clear signs or arthrosis/plates degeneration, vertebral apophysis alterations, signs of osteoporosis, and osteophites (usual patient subject to implant surgery). Note the important geometrical/radiological information that can be guessed and measured from this kind of image with the implementation of markers. In other words, the radiological experimental both *in vitro* and *in vivo* with markers, can provide practical information for implants design, since the markers define clearly the geometry of the implant at any position/shape-change. For experimental at lab, we used a different RX machine, a Siemens Siremovil 4K C-Arm RX machine screen with a simple radiological simulation of an artificial intervertebral disk with natural bones (cadaveric lumbar vertebras) and mixed tantalum markers (yellow/orange arrows, pictured, 60 Kvp and 1.2 mA x s). These markers (60% tantalum from Ref 9) can be used for imaging position determination [Ref 4]. This real clinical image could give an initial idea about the positioning of the markers, calculation of their geometry at screen of radioscopy machine/MRI, CT or conventional radiography imaging, and evaluation of the radio-opacity for further optimization. As said, for this experimental optimization at Lab, we used for the realistic radiological screen-photography of this type of simulations a Siemens Siremobil 4K, properly manufactured for surgical theatre. The lab work with C-Arm Siemens RX machine usually was made with the simplest settings for the C-Arm Siremobil. Kilvoltage selected was about 60 Kvp, and milliampereage 1.2mA.x s. The Tube Siemens was S02 Sirephos of 106 kVp and 30mA (Maximum values). That C-Arm machine has inherent filtration and also added filtration is possible.The C-Arm operated into the values of 60kV and 1.2mA x s, usually and the water tank was a thin-plastic of 45cm (w) x 30cm (h).According to all this, we selected two values of FSDs (focus-surface distances), ≈24 cm and ≈19cm. The corresponding VSDs (vertebrae-surface distances) were ≈9cm (for a water total thickness of 10cm) and ≈10 cm (for a water total thickness of 15cm). We refer the reader to [Ref 9] for extensive experimental details about markers optimization, both in radio-opacity and mixed-composition.Extent data about experimental optimization markers and stress/strain optimization according to selected markers geometry are detailed in [Casesnoves Ref 9 p].

$$\begin{pmatrix} \sigma_{X1} & \sigma_{Y1} & \sigma_{Z1} \\ \vdots & \vdots & \vdots \\ \vdots & \vdots & \vdots \\ \sigma_{X1} & \sigma_{Y1} & \sigma_{Z1} \end{pmatrix} = \begin{pmatrix} 1 & \left(\frac{\delta_{1X}}{L_X}\right) & \left(\frac{\delta_{1X}}{L_X}\right)^2 & 1 & \left(\frac{\delta_{1Y}}{L_Y}\right) & \left(\frac{\delta_{1Y}}{L_Y}\right)^2 & 1 & \left(\frac{\delta_{1Z}}{L_Z}\right) & \left(\frac{\delta_{1Z}}{L_Z}\right)^2 \\ & \vdots & \vdots & & \vdots & \vdots & & \vdots & \vdots \\ & \vdots & \vdots & & \vdots & \vdots & & \vdots & \vdots \\ 1 & \left(\frac{\delta_{nX}}{L_X}\right) & \left(\frac{\delta_{nX}}{L_X}\right)^2 & 1 & \left(\frac{\delta_{nY}}{L_Y}\right) & \left(\frac{\delta_{nY}}{L_Y}\right)^2 & 1 & \left(\frac{\delta_{nZ}}{L_Z}\right) & \left(\frac{\delta_{nZ}}{L_Z}\right)^2 \end{pmatrix} \times \begin{pmatrix} p(0)_{X1} & 0 & 0 \\ p(1)_{X1} & 0 & 0 \\ p(2)_{X1} & 0 & 0 \\ 0 & p(0)_{Y1} & 0 \\ 0 & p(1)_{Y1} & 0 \\ 0 & p(2)_{Y1} & 0 \\ 0 & 0 & p(0)_{Z1} \\ 0 & 0 & p(1)_{Z1} \\ 0 & 0 & p(2)_{Z1} \end{pmatrix}$$

MATRICES,3D AND 2D, FOR COMPUTATIONAL SIMULATIONS OF EQUATION RESULTS

$$\begin{pmatrix} \sigma_{X1} & \sigma_{Y1} \\ \vdots & \vdots \\ \vdots & \vdots \\ \sigma_{X1} & \sigma_{Y1} \end{pmatrix} = \begin{pmatrix} 1 & \left(\frac{\delta_{1X}}{L_X}\right) & \left(\frac{\delta_{1X}}{L_X}\right)^2 & 1 & \left(\frac{\delta_{1Y}}{L_Y}\right) & \left(\frac{\delta_{1Y}}{L_Y}\right)^2 \\ & \vdots & \vdots & & \vdots & \vdots \\ & \vdots & \vdots & & \vdots & \vdots \\ 1 & \left(\frac{\delta_{nX}}{L_X}\right) & \left(\frac{\delta_{nX}}{L_X}\right)^2 & 1 & \left(\frac{\delta_{nY}}{L_Y}\right) & \left(\frac{\delta_{nY}}{L_Y}\right)^2 \end{pmatrix} \times \begin{pmatrix} p(0)_{X1} & 0 \\ p(1)_{X1} & 0 \\ p(2)_{X1} & 0 \\ 0 & p(0)_{Y1} \\ 0 & p(1)_{Y1} \\ 0 & p(2)_{Y1} \end{pmatrix}$$

Matrix Algebra Formulation 1. Comparative Matrix Algebra Polynomial formulation for inverse numerical fitting of stress and strain contact mechanics magnitudes , both in 2D and 3D.The matrix of contact mechanics to carry out the numerical approximation (second degree polynomial), instead the linear equation that links stress and strain with the E modulus, is shown. Computational framework was done with Freemat 4.2. Although 3D matrix seems to be large and difficult, programming software does not result complicated.

Table 3. The basic geometrical units that can be used both for determination of IRC/IAR/HAR and engineering design of the implants and lumbar intervertebral disks. These geometrical/CAD concepts and techniques can be applied for IRC/IHA determination through imaging method

Basic geometrical concepts for geometrical-imaging/radiology and imaging CAD			
Geometrical unit	**Application element**	**Geometrical application**	**Comments**
Point	2D/3D spatial point	Large number of imaging applications	Basic unit in CAD, computing to build others
Line	NURBS of all types	Surface CAD and CAD design mainly	Good classical method in constructive approximation
Triangle	Delaunay triangulation	Surface cad and cad design mainly pixelization	Good method in continuous improvements
Tetrahedral prism (regular/irregular)	Voxelization minimum volume	CAD mechanics design,volume design,dynamics/kinematics of solids,rigid and deformable	This is the basic unit in volume optimization
Parallelepipedic volume regular/irregular	Voxelization for volume	CAD mechanics design,volume design,dynamics/kinematics of solids,rigid and deformable	4-points define volume that can be decomposed into tetrahedral prisms

Table 4. [from ref 6] we show the numerical results for a 2D simulation of implant of size (a,b,c) where areas of stress and strain are A1 = ab and A2 = bc , 2 height, 2 long, and 1 width (any unity).The IRC selected is different for each angle (see angle range). The loads applied are standard for lumbar spine simulations, from 78 N to 488 N [refs 5,6].Loads are used to calculate stress and deformations to implement values into the polynomial fitting.

Inverse 2D Simulations From References, Exact Solutions, Algorithm With Minimization Derivatives									
Angle	**IRC selected**	**IRC natural**	**Deformation Pixel 1** ε_1 ε_2	**Deformation Pixel 2** ε_1 ε_2	**IRC approx Pixel 1**	**IRC approx Pixel 2**	**IRC error Pixel 1**	**IRC error Pixel 2**	**Comments**
20	$(2.5,2.5)^T$	$(2,2)^T$	(0.1440,-0.7737)	(-0.1628,-0.2767)	(2.5001,2.4247)	(2.6989,2.5000)	10^{-3}	10^{-3}	
20	$(2.2,2.2)^T$	$(2,2)^T$	(0.0495,-0.6018)	(-0.0225,-0.1562)	(0.1787,2.2000)	(2.2000,2.2000)	10^{-4}	10^{-6}	
50	$(1.8,1.8)^T$	$(2,2)^T$	(-0.0065,-0.0273)	(0.0856,-0.2034) for 2 we vary coordinate y	(1.8000,1.7999)	(1.8002,1.7998)	10^{-5}	10^{-3}	Almost Exact Data Got
50	$(2.3,2.3)^T$	$(2,2)^T$	(0.0118,0.4467)	(-0.2138,-0.7982)	(2.2995,2.3000)	(2.2999,2.3000)	10^{-4}	10^{-5}	Almost Exact Data Got
50	$(1.7,1.7)^T$	$(2,2)^T$	(-0.0095,-0.4034)	(0.1211,-0.2943)	(1.7003,1.6983)	(1.7003,1.6993)	10^{-4}	10^{-4}	
AVER -AGE	N/A	N/A	N/A	N/A	N/A	N/A	10^{-4}	10^{-4}	

Table 5. [from ref 6] we show the numerical results for a 3D simulation of implant of size (a,b,c) where areas of stress and strain are A1 = ab and A2 = bc , 2 height, 2 long, and 1 width (any unity).The IRC selected is different for each angle (see angle range). The loads applied are standard for lumbar spine simulations, from 78 N to 488 N [refs 5,6]. Loads are used to calculate stress and deformations to implement values into the polynomial fitting.

Inverse 3D Simulations From References, Exact Solutions, Algorithm with Linear Equation System Programming						
Euler rotation angles θ around z α around y (in this order)	**IRC natural**	**IRC selected**	**IRC linear system exact solution**	**Deformations Voxel 1 In X In Y In Z** $\varepsilon_{1=1}^{st}$ **Equation** $\varepsilon_{2=2}^{nd}$ **Equation** $\varepsilon_{3=3}^{rd}$ **Equation**	**Deformations Voxel 2 In X In Y In Z** $\varepsilon_{1=1}^{st}$ **Equation** $\varepsilon_{2=2}^{nd}$ **Equation** $\varepsilon_{3=3}^{rd}$ **Equation**	**Inverse Problem Magnitude Order Voxel 1 Voxel 2**
θ=30	X=1	X=1.5	X=1.5000	ε1 =-0.2531	ε1 =+1.0183	10^{-4} (2) 10^{-2}
α=40	Y=1	Y=1.5	Y=1.5002	ε2 =+0.1492	ε2 =-0.2940	
	Z=1	Z=1.5	Z=1.5001	ε3 =+0.3984	ε3 =+0.3839	
θ=30	X=1	X=1.4	X=1.4	ε1 =-0.2265	ε1 =-0.0236	10^{-1} (2) 10^{-2}
α=40	Y=1	Y=1.4	Y=1.4	ε2 =+0.1147	ε2 =-0.2054	
	Z=1	Z=1.4	Z=1.4	ε3 =+0.3092	ε3 =+0.2936	
θ=40	X=1	X=2	X=2	ε1 =-0.8464	ε1 =-0.9231	10^{-1} (2) 10^{-2}
α=30	Y=1	Y=2	Y=2	ε2 =+0.6989	ε2 = 1 (*)	
	Z=1	Z=2	Z=2	ε3 =+1.3238	ε3 =+0.6382	
θ=40	X=1	X=1.5	X=1.5	ε1 =-0.6824	ε1 =+0.5331	10^{-1} (2) 10^{-2}
α=30	Y=1	Y=1.5	Y=1.5	ε2 =+0.2721	ε2 = 2 (*)	
	Z=1	Z=1.5	Z=1.5	ε3 =+0.5859	ε3 =+0.2470	
Average Error Magnitude	N/A	N/A	N/A	ABOUT 10^{-1}	ABOUT 10^{-1}	ABOUT 10^{-2}

Inverse 3D Simulations From References, Exact Solutions, Algorithm with Linear Equation System Programming						
Euler rotation angles θ around z α around y (in this order)	**IRC natural**	**IRC selected**	**IRC linear system exact solution**	**Deformations Voxel 1 In X In Y In Z $\varepsilon_{1=1}$st Equation $\varepsilon_{2=2}$nd Equation $\varepsilon_{3=3}$rd Equation**	**Deformations Voxel 2 In X In Y In Z $\varepsilon_{1=1}$st Equation $\varepsilon_{2=2}$nd Equation $\varepsilon_{3=3}$rd Equation**	**Inverse Problem Magnitude Order Voxel 1 Voxel 2**
Comments				1(*) ε1 =+0.2798 ε2 =+0.2192 ε3 =-0.1426	2(*) ε1 =-0.7202 ε2 =-0.1232 ε3 =-1.5704	Data is almost exact, in1,2(*) all coordinates were varied

Table 6. Pictured, [Ref 8 p, implemented with new software and setting numerical approximations by intervals], the numerical results for a 3D simulation of implant of two voxels of Fig 5 with matrix of numerical method in 3D, Table 2. This primary approximation shows the real numerical application of the inverse problem to determine a deformation and posterior numerical non-linear equations for 2 voxels.

Computational results for 3d simulations with 2 voxels		
IRC natural	**IRC selected**	
(1,1,1)	**(1.5,1.5,1.5) and (1.4,1.4,1.4) equations are approximated for both IRCs**	
Comments For equations	**Last term negative is the most important**	
Numerical equation stress/strain		**Load interval (N)**
$\sigma_{1X} = 105.1416 + 412.4233\ (\varepsilon_{1X}) - 826.9638\ (\varepsilon_{1X})^2$;		
$\sigma_{1Y} = 30.6659 + 121.1546\ (\varepsilon_{1Y}) - 242.9318\ (\varepsilon_{1Y})^2$;		[78, 181]
$\sigma_{1Z} = 72.3484 + 283.7889\ (\varepsilon_{1Z}) - 569.0360\ (\varepsilon_{1Z})^2$;		
$\sigma_{1X} = 218.6980 + 412.4223\ (\varepsilon_{1X}) - 826.9640\ (\varepsilon_{1X})^2$;		
$\sigma_{1Y} = 63.2859 + 133.4428\ (\varepsilon_{1Y}) - 267.5713\ (\varepsilon_{1Y})^2$;		[282, 385]
$\sigma_{1Z} = 150.4870 + 283.7890\ (\varepsilon_{1Z}) - 569.0360\ (\varepsilon_{1Z})^2$;		
$\sigma_{1X} = 276.0328 + 412.4215\ (\varepsilon_{1X}) - 826.9624\ (\varepsilon_{1X})^2$;		
$\sigma_{1Y} = 79.8640 + 119.0563\ (\varepsilon_{1Y}) - 238.7245\ (\varepsilon_{1Y})^2$;		[385, 488]
$\sigma_{1Z} = 189.9384 + 283.7834\ (\varepsilon_{1Z}) - 569.0221\ (\varepsilon_{1Z})^2$;		
CONCLUSIONS		
We used 2 similar IRCs for inverse problemDeformation was applied for several loads intervals		Equations constitute an initial approximation for 2 voxels

Table 7. [from ref 6 3D, Voxels 1 and 2] we show the numerical results for a 3D simulation of implant of size (a,b,c) where areas of stress and strain are A1 = ab and A2 = bc , 2 height, 2 long, and 1 width (any unity).Angles of Rotation are especified. The IRC selected is different for each angle (see angle range). The loads applied are standard for lumbar spine simulations, from 78 N to 488 N [refs 5,6]. Loads are used to calculate stress and deformations to implement values into the polynomial fitting. Voxels are according to Fig 5.

Initial simulation data from references 3D flexion and lateral bending		
Voxel/element	**Initial points and rotation angles**	**Final points and rotation angles**
VOXEL/ELEMENT 1	Voxel-1 α = 30 θ = 40	Voxel-1 α = 30 θ = 40
	(-1, 2, 1)	(-0.0500, 2.1748, 1.1258)
	(1, 3, 1)	(1.8335, 1.6550, 2.2132)
	(1, 3, 0)	(2.3335, 1.6552, 1.3472)
	Voxel-1 α = 40 θ = 30	Voxel-1 α = 40 θ = 30
	(-1, 2, 1)	(-0.5222, 2.2320, 0.8521)
	(1, 3, 1)	(1.1696, 2.0980, 2.2869)
	(1, 3, 0)	(1.8124, 2.0980, 1.5209)
VOXEL/ELEMENT 2	Voxel-2 α = 30 θ = 40	Voxel-2 α = 30 θ = 40
	(-1, 1, 1)	(-0.5067, 2.9408, 1.4472)
	(1, 1, 1)	(0.7201, 0.1232, 1.5704)
	(1, 2, 0)	(1.7768, 0.8892, 1.0258)
	Voxel-2 α = 40 θ = 30	Voxel-2α = 40 θ = 30
	(-1, 1, 1)	(-0.9232, 13660, 0.5307)
	(1, 1, 1)	(0.4036, 0.3660, 1.6441)
	(1, 2, 0)	(1.4294, 1.2320, 1.1995)

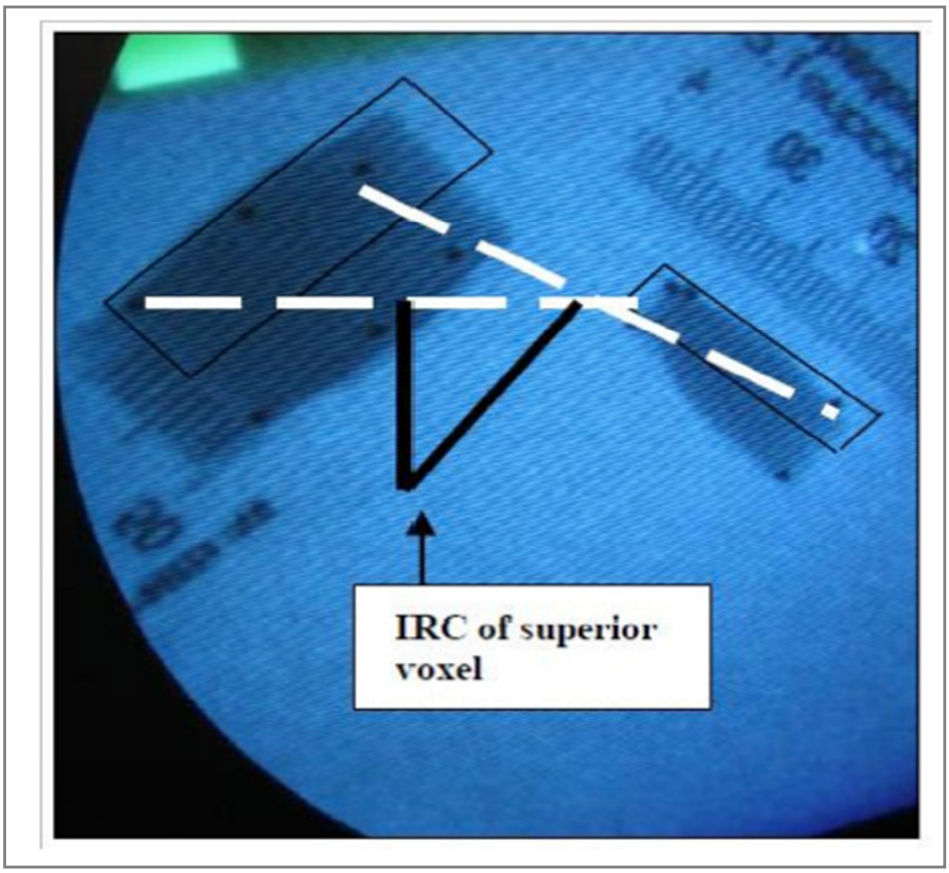

Fig. 10. Radiological Simulation for IRC approximate Determination with Implant Deformation. A compliant artificial disk manufactured with composites and its radiological simulation for an exaggerated lumbar spine flexion-compression. These markers (Mixed Tantalum 60% from ref 7, principal) can be used for imaging position determination [ref 7]. We used, as said, for the realistic radiological screen-photography of this simulation a Siemens Siremobil 4K, C-Arm RX-Machine properly manufactured for surgical theatre. Distances are measured with a radiological rule that appears in image. This type of radiological apparatus are used in surgery to fit exactly the position of the artificial implant. The mechanical reason is that the arm of the machine can be moved along several angles/distances, in such a way that avoiding surgical sterilized blanketts and covers, or any anatomical part of the patient which is hindering the imaging-geometrical setting for good visualization at screen. In addition, in spinal surgery, and specially in lumbar disk pathology, it is not unfrequent to find obese patients who create radiological difficulties that can be overcome by the mechanical adaptation of this C-Arm machine. It was proven mathematically/simulations [Casesnoves,4,5,6,7], that the IRC/IAR of this implant can be approximated with these radiological imaging techniques using the Numerical Reuleaux Method. Furthermore, the precision of this IRC/IAR determination could be improved by using better imaging-radiological equipment, MRI or CT techniques, or standard radiological simulators [designed by Casesnoves, 2008, proceedings of SIAM Conference in Computational Science/Engineering, 2009].

References

[1] Casesnoves, F. '3D Improved Mathematical Model for Lumbar Intervertebral Ligaments (Lils)'. Peer-reviewed SIAM Poster. SIAM San Diego Life Sciences Conference. August 2012. San Diego, California, USA.

[2] Casesnoves, F. "An Optimization Method for anterior vertebral body morphometry to enhance surgical devices". Lecture-Poster. 2008 SIAM Conference of Imaging Science. San Diego CA, USA. July 2008. 2.1-Casesnoves, F." Computational Simulations of Anterior Vertebral Surface for Statistical Optimization in Surgical Instrumentation Design". ASME Peer-reviewed Conference Paper and Poster. Proceedings of the 2010 Design of Medical Devices Conference. April 13-15, 2010, Minneapolis, MN, USA.

[3] Casesnoves, F. "Spinal Biomechanics Mathematical Model For Lumbar Intervertebral Ligaments". 2011 SIAM Conference on Computational Science and Engineering. Reno, Nevada, USA.

[4] Casesnoves F. 'Simulations of the NRM for Lumbar Artificial Disc Implants IRC Determination' Casesnoves. SIAM Conference in Computational Science/Engineering. MI. USA. 2009.

[5] Casesnoves, F. ´Theory and Primary Computational Simulations of the Numerical Reuleaux Method (NRM)´ International Journal of Mathematics and Computation (http://www.ceser.in/ceserp/index.php/ijmc/issue/view/119). Volume 13, Issue Number D11.2011.

[6] Casesnoves, F. 'Applied Inverse Methods for Deformable Solid Dynamics/Kinematics in Numerical Reuleaux Method (NRM)' Casesnoves, F. International Journal of Numerical Methods and Applications. Volume 9(2) 2013 .Pages 109-131. Peer-Reviewed International Mathematical/Computation Journal Article Print/Online.http://www.pphmj.com/abstract/7688.htm.

[7] Bartholomew-Biggs, M. Nonlinear Optimization with Engineering Applications. Springer Optimization and its Applications. 2008.

[8] Casesnoves, F. Bioengineering Inverse Methods for Optimal Geometrical/Mechanical Deformation of Lumbar Artificial Disks/Implants Using the Numerical Reuleaux Method. Peer-reviewed Poster by international selected Chairs Panel. International Conference on Significant Advances in Biomedical Engineering. OMICS International Conference. Philadelphia April 2015. This Poster was officially awarded by Scientific Program Chairs Panel as the Best Poster Presentation at Conference, for scientific significance and bioengineering interest. Official Certificate, 28th April, 2015.

[9] Casesnoves, F. 'Experimental Optimization of Radiological Markers for Artificial Disk Implants with Imaging/Geometrical Applications. A Functional Manufacturing Basic'. Peer-reviewed article. Print and Online. Researches and Applications in Mechanical Engineering Vol 2 Issue 4.December 2013. http://seipub.org/rame/paperInfo.aspx?ID3913.

[10] Abramovitz, M, Stegún, I. Handbook of Mathematical Functions. Ninth Edition. 1970. Aparecido, H, De Padua, M, Shimano, A. 'Compression or Distraccion Forces Applied on a Pedicular Fixation System:An Experimental Study'.Acta Orthopedica Brasilera 14(3) – 2006.

[11] Bartholomew-Biggs, M. 'Nonlinear Optimization with Engineering Applications'. Springer Optimization and its Applications. 2008.

[12] Bertsekas, DP. 'Nonlinear Programming'. Second Edition. Athena Scientific. 2003.

[13] Casesnoves, F. 'Simulations of the Numerical Reuleaux Method (NRM) for Lumbar Artificial Disk Implants IRC Determination' Casesnoves. Peer-reviewed SIAM Poster. SIAM Conference in Computational Science/Engineering. MI. USA. 2009.

[14] Cheney, W., and Light, W., 2000, A Course in Approximation Theory (Graduate Studies in Mathematics), Am. Math. Soc., Providence, RI, Vol. 101.

[15] Christopher J. Colloca, DC, a and Richard N. Hinrichs. 'The Biomechanical and Clinical Significance of the Lumbar Erector Spinae Flexion-Relaxation Phenomenon: A Review of the Literature'. Journal of Manipulative and Physiological Therapeutics.October 2005.

[16] Gail, J M. 'Biomechanics of Lumbar Intervertebral Disk: A Review'. Phys. Ther. 1980; 60: 765-773.

[17] Crisco J, Fujita, Spenciner D. 'The dynamic flexion/extension properties of the lumbar spine in vitro using a novel pendulum system'. Journal of Biomechanics 40 (2007) 2767–2773.

[18] Hildebrand, F B. 'Introduction to Numerical Analysis'. Second Edition, revised. Dover Publications, Inc., 1987.

[19] Jaumar, N, and Colls. 'Contact Pressure in the Facet Joint During Sagittal Bending of the Cadaveric Cervical Spine'. Journal of Biomechanical Engineering. July 2011, Vol 133.2011.

[20] Kiefer, A, Shirazi, Adl, Parnianpour, M. 'Stability of the Human Spine in Neutral Postures'. Eur Spine J (1997). 6:45-53. Springer 1997. A

[21] Knudson Duane. 'Fundamentals of Biomechanics'. Second Edition. Springer 2007.

[22] Levangie, P, and Norkin, C. 'Joint Structure and Function: A Comprehensive Analysis'. Fourth Edition. F. A. Davis Company, Philadelphia. 2005.

[23] Maquer, G.' Image-based biomechanical assessment of vertebral body and intervertebral disc in the human lumbar spine'. Doctoral Thesis. Bern University. 2013.

[24] Medical Advisory Secretariat, Ministry of Health. 'Artificial Discs for Lumbar and Cervical Degenerative Disc Disease – Update An Evidence-Based Analysis. Ontario Health Technology Assessment Series 2006; Vol. 6, No. 10.

[25] O'Shaughnessy, Jean-François Roy J F and Martin Descarreaux M. 'Changes in flexion-relaxation phenomenon and lumbo-pelvic kinematics following lumbar disc replacement surgery'. Journal of Neuro Engineering and Rehabilitation 2013, 10:72.

[26] Palepu, V, Kodigudla M, and V. K. Goel, V K.'Biomechanics of Disc Degeneration'. Hindawi Publishing Corporation. Advances in Orthopedics. Volume 2012, Article ID 726210, 17 pages. doi: 10.1155/2012/726210.

[27] Rousseau, M-A, Bradford, DS, Hadi TM, Pedersen KL, and Lotz JC.'The instant axis of rotation influences facet forces at L5/S1 during flexion/extension and lateral bending'.Eur Spine J. 2006 Mar; 15(3): 299–307.

[28] Wachowski, and 9 collaborators. 'Migration of the instantaneous axis of motion during axial rotation in lumbar segments and role of the zygapophysial joints'. Acta of Bioengineering and Biomechanics.Vol. 12, No. 4, 2010.

[29] White, A., and Panjabi, M., 1978. 'Clinical Biomechanics of the Spine'. J. B. Lippincott & Co., Philadelphia, PA.